Static and dynamic aspects of coupling between creep behavior and oxidation on MC2 single crystal superalloy at 1150 °C

Sébastien Dryepondt[a], Daniel Monceau[a, 1], Fabrice Crabos[b] and Eric Andrieu[a]

[a]CIRIMAT UMR 5085, ENSIACET-INPT, 31077 Toulouse Cedex 4, France

[b]TURBOMECA, 64511 Bordes, France

Abstract

Creep tests were performed on thin wall specimens made of MC2 single crystal superalloy at 1150 °C and under controlled atmosphere. The results highlight the deleterious oxidation effect on creep properties. The assumption that oxidation leads to a non-load-bearing affected zone is insufficient to explain the difference in creep rate that was noticed between tests performed under synthetic air and under hydrogenated argon, and cannot explain the decrease of the strain rate during the tests that were carried out with a change of atmosphere from synthetic air to hydrogenated argon. On the other hand, these experimental results are consistent with vacancy injection due to partial cationic oxidation, which accelerates the creep rate by promoting creep mechanisms controlled by diffusion. The anionic protective alumina scale formed under hydrogenated argon prevents this vacancy flux. The integration of this dynamic and long range oxidation effect in creep strain models is discussed.

Keywords: Creep test; Controlled atmosphere; Nickel alloys; Oxidation; High temperature deformation

1. Introduction
2. Materials and experimental procedures
2.1. Materials
2.2. Creep tests
2.3. Thermogravimetric tests
3. Results
3.1. Influence of environment on creep properties
3.2. Characterization of the affected zone
3.2.1. Thermogravimetric tests
3.2.2. Creep tests specimen
3.2.3. Effect of the depleted zone on the creep rate
3.3. Dynamic effect of oxidation on creep properties
3.3.1. Change from ArH2 to synthetic air
3.3.2. Change from synthetic air to ArH2
4. Discussion
4.1. Stress effect on the oxide growth
4.2. Oxidation effect on the creep properties of the single crystal superalloy
4.3. Comments on creep curves obtained according to the atmosphere
4.3.1. Primary creep stage
4.3.2. Steady state creep stage
4.3.3. Tertiary creep stage

1. Introduction

Lifetime prediction of structural components loaded mostly in axial tension relies on a set of data obtained from standard creep testing. The stress state in the section of the tested specimen is assumed to be uniform and the global mechanical response of the sample is considered representative of the behavior of a volume element of the mechanics of continuous media. Fortunately, these assumptions are valid in most cases. However, when there are interactions between the environment and the alloy, the validity of the usual creep test analysis has to be reconsidered. When creep tests are conducted under severe oxidation and/or corrosion conditions, the mechanisms related to the oxide scale growth can affect the alloy microstructure stability. The consequent microstructural changes, in the grains or along grain boundaries, are likely to generate a mechanical properties gradient from the alloy surface to the bulk material [1], [2], [3] and [4]. Although the characterization of the affected zone may be hard, the estimation of its relative extent, based often on diffusion models, gives useful information to go along with the creep test analysis. Thus, the composite model proposed by Dyson and Obgerby [5], with the consideration of a new material developing at the alloy surface, has proved to be appropriate in many cases, from a hardening adherent oxide to a deleterious non-load-bearing affected zone [6] and [7]. However, several studies demonstrated that the microstructure can be affected by longer range oxidation effects, such as vacancy injection [3], [4], [8] and [9], or the formation of new phases because of selective oxidation [10]. In this case, the relevance of the previous kinds of models has to be discussed.

The aim of the present study is first to highlight the oxidation effect on the creep properties of a single crystal Ni-based superalloy. In order to achieve this objective, the environment was carefully controlled and thin wall creep specimens were chosen to get a sufficiently high ratio between the oxidation exposed surface and the total volume of the specimen [11], [12] and [13]. Thicknesses used were still thick enough to keep the engineering properties (σ_{ys}, σ_{uts}) unchanged up to 1150 °C.

Particular attention was paid to the morphology and the microstructure of the oxides as well as to the depth of the corresponding microstructural evolution of the metallic substrate. Then, the relevance of the convenient assumption of the existence of an equivalent non-load-bearing zone is reexamined in this particular case. Finally, specific creep tests with a sudden environment change were carried out with the objective of estimating the relative amplitude of dynamic oxidation effects on creep strain rate.

2. Materials and experimental procedures

2.1. Materials

Thin sheets of 1.2 mm thickness were cut from heat-treated single crystal plates made of MC2 alloy (cf. Table 1), and were then ground to 1 mm. Thin creep specimens were then machined by spark erosion so that the loading axis is parallel to the longitudinal [0 0 1] direction of these sheets. They were mechanically polished with SiC paper and diamond paste down to 3 μm to remove the thin oxide layer developed during grinding.

Table 1.

Chemical composition of MC2 alloy (wt.%)

Ni	Cr	Co	Al	Mo	Ti	W	Ta
Bal.	7.8	5.2	5	2.1	1.5	8	5.8

2.2. Creep tests

Creep tests were carried out at 1150 °C under hydrogenated argon (argon + 5 vol.% H_2) and synthetic dry air on a MTS electromechanical machine equipped with a specifically developed environmental setup. The specimens were heated by a radiation furnace which allows high heating and cooling rates. Three "S" thermocouples were spot welded: one in the middle of the gauge length to regulate the temperature (±2 °C) and the other two to estimate the thermal gradient. Glass windows let a laser beam go through the furnace and therefore allow measurement of the displacement between two L-flags that were spot welded on the gauge length. Specimen geometry and flags location are shown in Fig. 1.
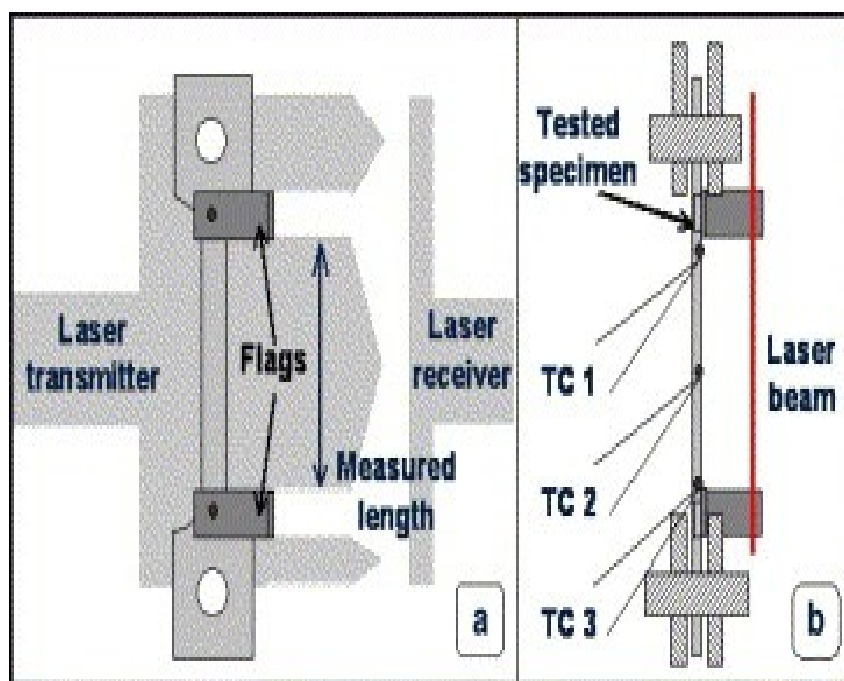

Fig. 1. Specimen geometry with flags and thermocouple locations: (a) front view of the tested specimen and location of the laser beam; (b) side view of the assembly.

Creep tests were carried out up to rupture under synthetic dry air and hydrogenated argon at 1150 °C, with an applied stress σ_0 which was chosen so that $\sigma_0/\sigma_{uts} \approx 1/3$. σ_{uts} is the ultimate tensile strength that was obtained from a tensile test performed at 1150 °C and a strain rate of 10^{-3} s^{-1}.

2.3. Thermogravimetric tests

Oxidation tests were performed with an automatic recording thermobalance SETARAM TAG 24S equipped with a double symmetrical furnace which provides a very stable signal and minimizes the drift error to less than 1 μg for a test duration of 24 h. The temperature, atmospheres and test durations were chosen to be the same as for the creep tests. The parabolic rate constants were calculated using the method described in [14]. This method also allows the estimation of a rate constant during the transient oxidation stage.

3. Results

The different creep curves obtained have been analyzed and compared according to the atmosphere. Microstructural observations of the specimens, especially in the area close to the surface, were carried out to find out how the oxidation affects the creep properties of the superalloy.

3.1. Influence of environment on creep properties

The environmental effect on the superalloy creep behavior is clearly illustrated by the creep curves presented in Fig. 2. The light gray curve corresponds to the test performed at 1150 °C under synthetic air, and the dark one corresponds to the same test but under hydrogenated argon. These two curves are similar up to the establishment of the steady state creep stage in synthetic air. Under hydrogenated argon, the creep rate keeps on decreasing, and this leads to a ratio of 5 between the minimum creep rate under synthetic air and in hydrogenated argon. The duration of the steady state stage is then 3 times longer under hydrogenated argon than synthetic air but the tertiary stage starts for a deformation of 0.65%, whatever the atmosphere is.
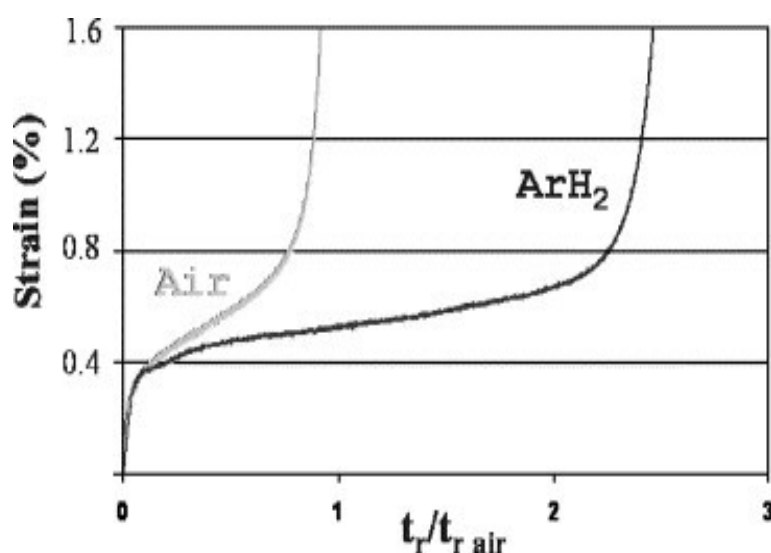
Fig. 2. Creep curves resulting from tests performed at 1150 °C in hydrogenated argon and in synthetic air.

In Fig. 3, the creep strain rate is plotted versus true stress in a bilogarithmic diagram, by considering an homogeneous section decrease due to the uniform deformation of the specimen. The curve shapes obtained after creep tests under synthetic air and hydrogenated argon are close and one can notice again that the minimum creep rate is lower under hydrogenated argon. Previous tests were performed on the same kind of specimen to estimate the values of the parameters $\dot{\varepsilon}_0$ and N in the Norton power law: $\dot{\varepsilon} = \dot{\varepsilon}_0 \left(\frac{\sigma}{\lambda}\right)^N$ at 1150 °C. Thus, the dotted line in Fig. 4 represents the linear relation $\log \dot{\varepsilon} = N \cdot \log \sigma$.
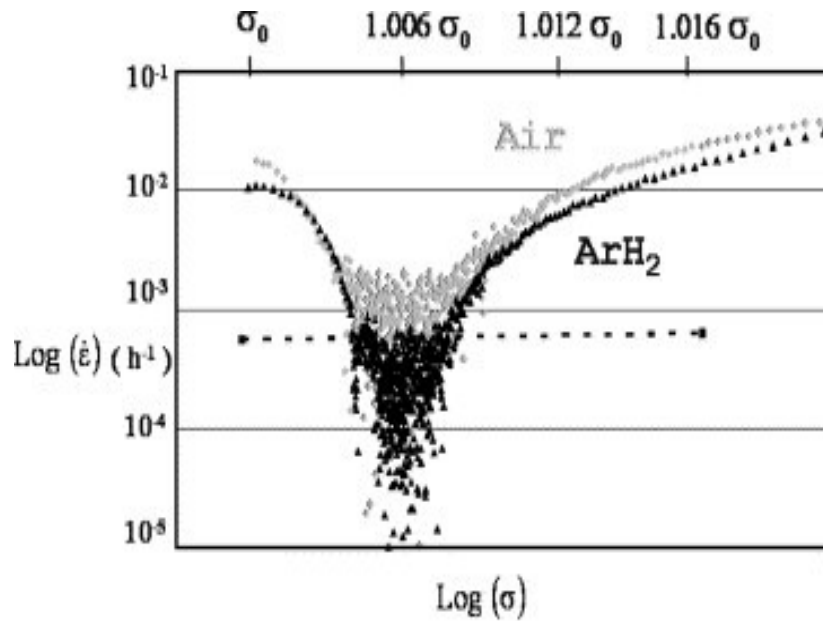

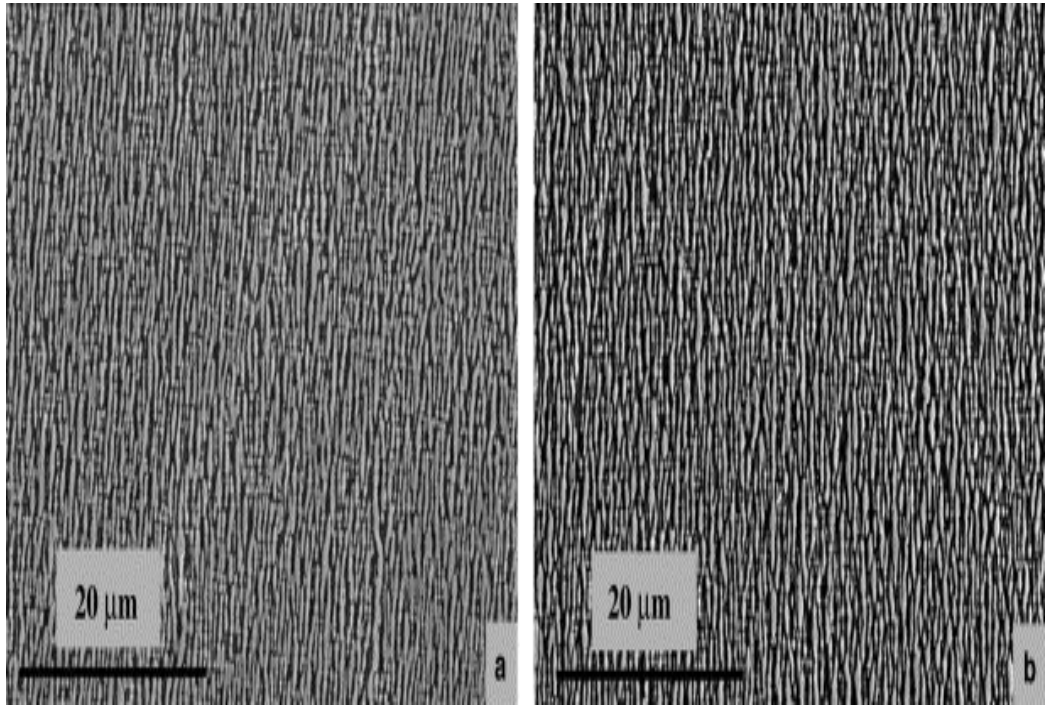Fig. 3. Creep rate versus stress in a bilogarithmic diagram.

Fig. 4. Post-mortem SEM micrographs of the bulk material: (a) specimen crept under synthetic air; (b) specimen crept under hydrogenated argon.

At the beginning of the tertiary stage, the trend lines of the two curves are very far from the dotted line. This behavior suggests that the tertiary creep is not due to the section decrease because of the specimen deformation, but to a severe degradation of the superalloy. Thus, the Norton power law is no longer applicable at this stage.

The micrographs of Fig. 4 prove that the microstructural evolution far from the necking zone is similar under synthetic air and hydrogenated argon, whereas the creep test duration was 2.5 times longer under hydrogenated argon than under synthetic air. The similar microstructures in the necking zone (Fig. 5) indicate that the damage mechanisms remain the same too.
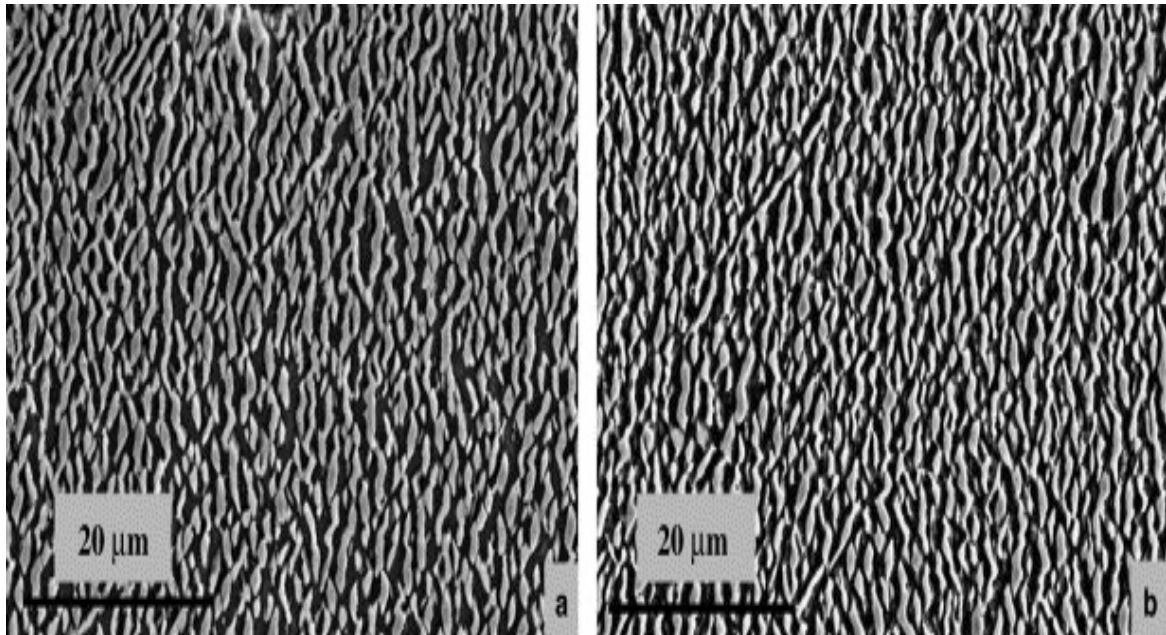
Fig. 5. Post-mortem SEM micrographs of the bulk material in the necking zone: (a) specimen crept under synthetic air; (b) specimen crept under hydrogenated argon.

3.2. Characterization of the affected zone

The usual way to study the kinetics of oxidation together with the oxidation effect on alloy microstructure is to perform thermogravimetric tests. However, there is no applied load on the material during this kind of test. Since the type of oxide and the kinetics of growth are susceptible to dependence on the stress state and deformation in the alloy, observations of the oxide scales and the affected zones after creep tests and thermogravimetric tests should be compared.

3.2.1. Thermogravimetric tests

The parabolic rate constants, calculated from the steady state stages of the mass gain curves (Fig. 6(a)), are the same for the two tested atmospheres (Fig. 6(b)), although the oxide layer grows faster during the transient stage under synthetic air than under hydrogenated argon (Fig. 6(a)). The estimation of the transient parabolic rate constants leads then to a higher value under synthetic air (Fig. 6(b)).
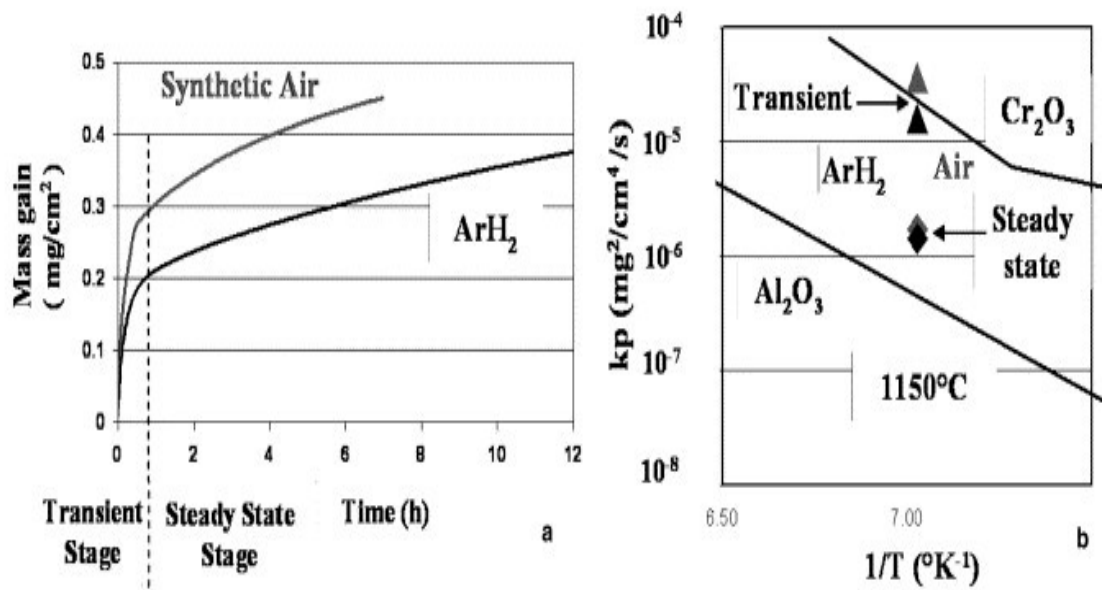
Fig. 6. (a) Mass gain curves resulting from thermogravimetric tests under hydrogenated argon and synthetic air at 1150 °C; (b) calculated k_p from the mass gain curves plotted in an Arrhenius diagram.

Under both atmospheres, the steady state stage corresponds to the growth of a smooth or slightly wrinkled alumina scale, about 3 μm thick after 7.3 h. In the micrographs of Fig. 7 and Fig. 8, one can observe smaller oxide grains at the surface of the alumina scale. Under synthetic air only, there are local clusters of oxides that are rich in Ni or Ti (Figs. 7(b) and (d)). This is probably the reason why there is a mass gain difference between the two atmospheres during the transient state stage
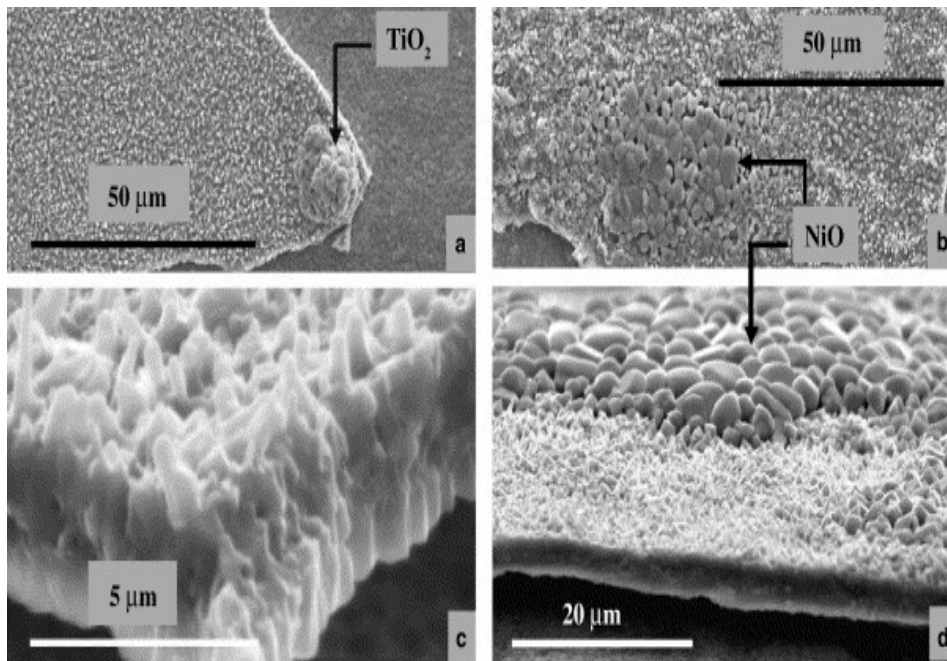
Fig. 7. Micrographs of the oxide layer after oxidation (1150 °C, 7.3 h) under synthetic air: (a) alumina scale with clusters of TiO_2; (b) alumina scale with clusters of NiO; (c) side view of the alumina scale; (d) side view of the alumina scale showing large NiO grains on the external part of the oxide scale.
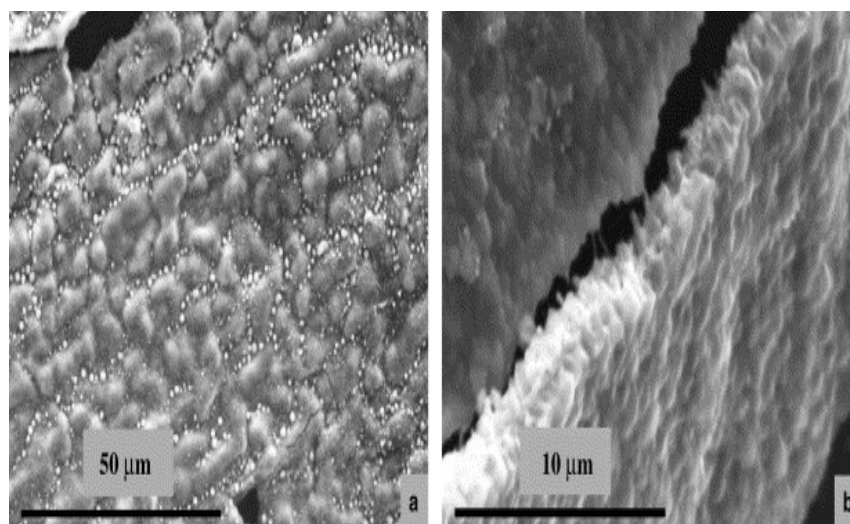

Fig. 8. Micrographs of the oxide layer after oxidation (1150 °C, 23 h) under hydrogenated argon: (a) surface of the alumina scale with small grains of other oxides; (b) broken alumina oxide scale showing the internal microstructure.

The consumption of aluminum to form the alumina oxide scale leads to the disappearance of γ' precipitates [15]. The thickness of the γ' depleted zones after thermogravimetric tests under synthetic air and hydrogenated argon is about 12 μm. This result is consistent with the fact that the mass gain during both oxidation experiments is similar, although the test duration is nearly 3 times longer under hydrogenated argon (see Fig. 9).
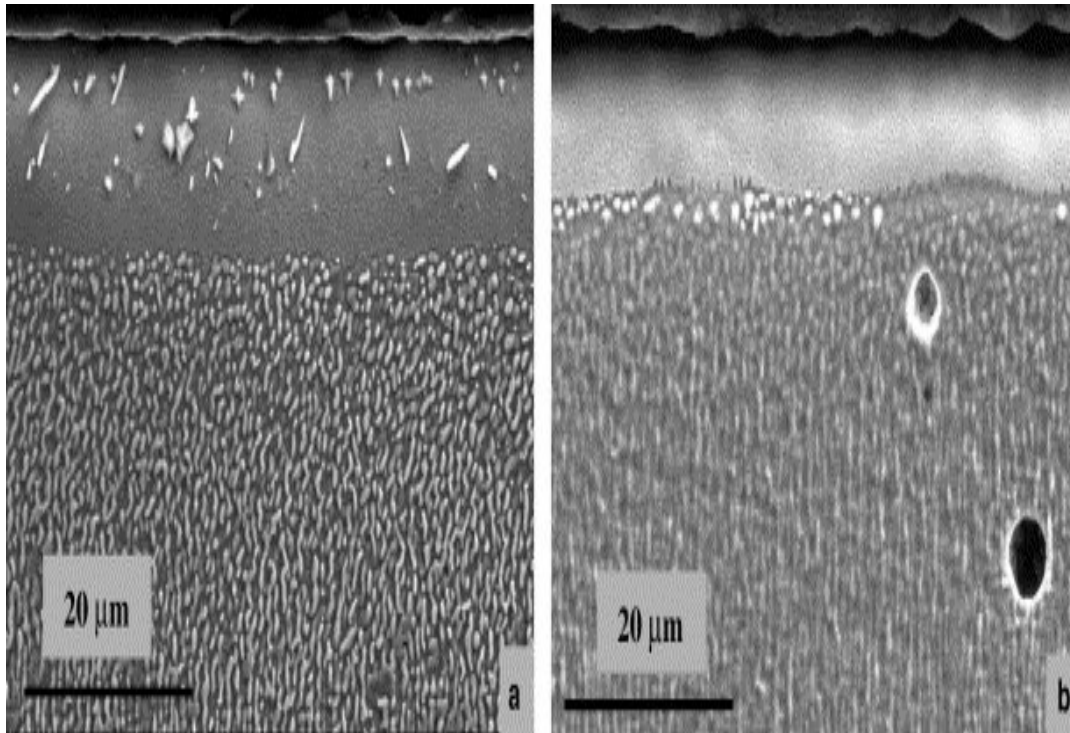

Fig. 9. Cross-section micrographs of the depleted zone after thermogravimetric tests: (a) after 7 h under synthetic air; (b) after 18 h under hydrogenated argon.

The mechanical properties of single crystal superalloy are known to be very dependent on the γ' volume fraction and the γ' precipitates morphology [16] and [17]. Thus, one can expect that the γ' depleted zone has a very weak creep resistance and, at this stage, the assumption of an affected non-load-bearing zone seems to be consistent with the first creep results, and has to be examined in detail.

3.2.2. Creep tests specimen

The micrographs presented below come from the observation of specimens after creep testing under controlled atmosphere.

The comparison of the micrographs of Fig. 8 and Fig. 10 reveals that the oxide layers formed under hydrogenated argon, with or without mechanical loading and for the same duration, are similar: both layers are dense and have the same thickness (3 μm), slightly wrinkled, and mainly composed of alumina. The resulting depleted zones are 10 μm thick.
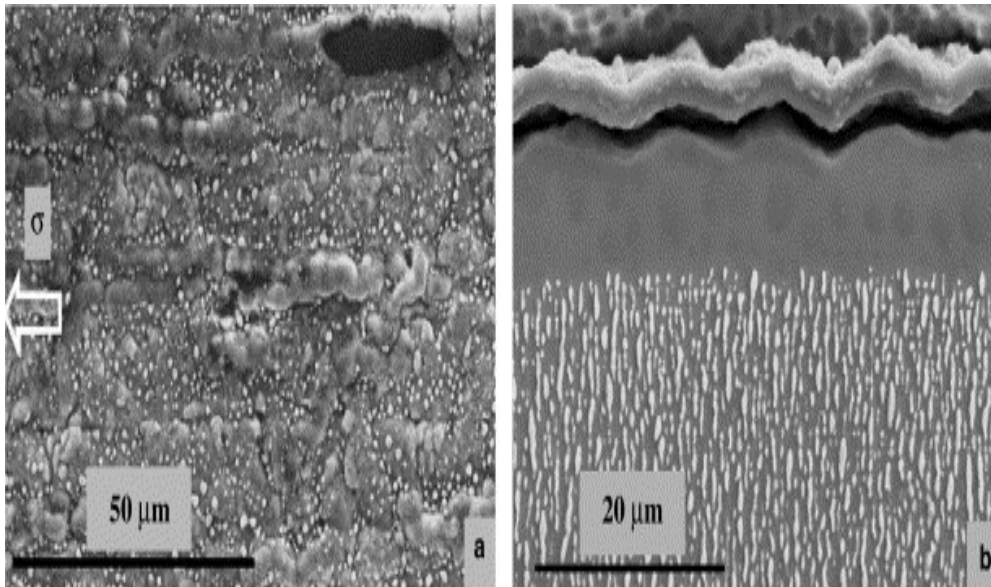
Fig. 10. Micrographs of the specimen after creep at 1150 °C-σ_0 MPa in hydrogenated argon: (a) overview of the oxide surface; (b) cross-section view of the depleted zone and of the oxide layer.

On the contrary, it appears obvious on the micrographs of Fig. 7 and Fig. 11 that the oxide scale grown under synthetic air depends on the applied stress. Two kinds of oxide scales were observed after creep testing: the first one is a wrinkled layer composed almost entirely of alumina (Fig. 11(a)). Note that the direction of the applied stress, which was also the direction of grinding, is a preferred axis for wrinkling. The second one is a less wrinkled scale but lots of oxides other than alumina were detected at its surface (Fig. 11(b)). The depleted zone varies on average from 15 to 20 µm (Fig. 12(a)). However, in regions where oxidation is highly developed, the affected zone may reach a thickness of 60 µm (Fig. 12(b)). These scanning electron microscopy (SEM) observations clearly demonstrate that the applied stress disturbs the oxide scale growth under synthetic air. The consequence is weak on the average depleted zone thickness but locally the γ' depleted zone developed during creep testing may be 6 times thicker than the one observed after thermogravimetric testing. The conclusion is that the microstructural changes at the surface of the specimen due to annealing are not always representative of microstructural changes after creep tests, even if temperature, atmosphere, and test duration are the same.

Fig. 11. Micrographs of the oxide layer surface of the specimen after creep at 1150 °C-σ_0 MPa under synthetic dry air: (a) area with a convoluted alumina layer; (b) area less convoluted with other oxides than Al_2O_3.
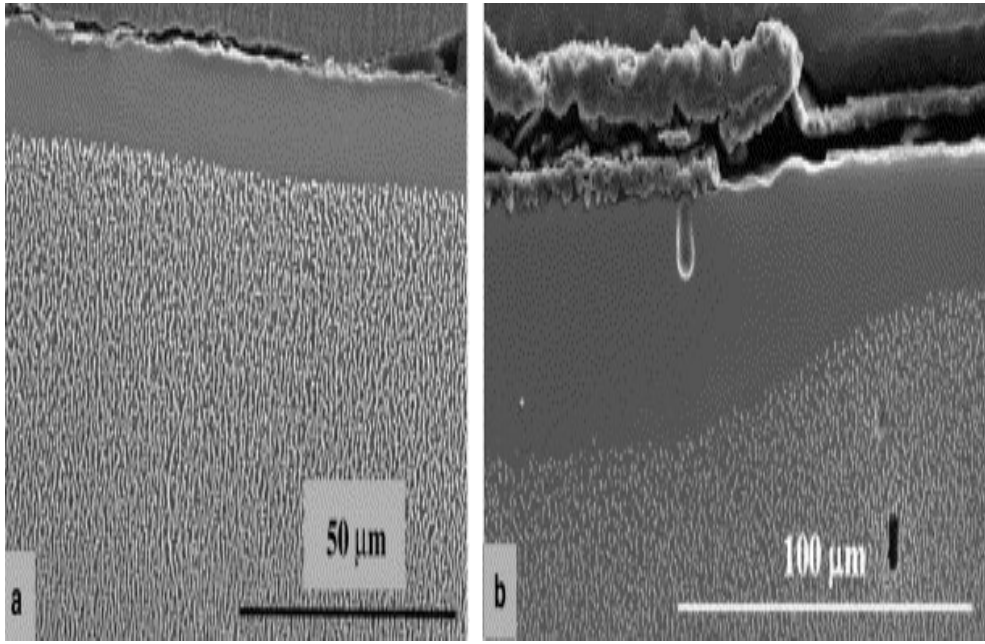
Fig. 12. Micrographs of the sample after creep at 1150 °C-σ_0 MPa under synthetic air: (a) general view of the depleted zone; (b) area with a change of depleted zone thickness due to a difference in oxide scale morphologies and compositions.

3.2.3. Effect of the depleted zone on the creep rate

As mentioned before, the γ' depleted zone leads to a decrease of the load-bearing section of the specimen, equivalent to an increase of the applied stress. In the case of a uniform depleted zone with a constant thickness e (Fig. 13), calculation of the effective stress σ' ends up to the equation:

(1)
$$\sigma' = \frac{\sigma \cdot S}{S'} \approx \frac{\sigma}{1 - \alpha \cdot e} \quad \text{with } \alpha = \frac{\text{perimeter}}{\text{section}}.$$

Using the appropriate Norton flow law, the minimum creep rate is then given by the equation:

(2)
$$\dot{\varepsilon} = \dot{\varepsilon}_0 \left(\frac{\sigma}{1 - \alpha \cdot e} \right)^N.$$

For the same test time at high temperature, the γ' depleted zone is thicker under synthetic air than under hydrogenated argon. This difference of γ' depleted zone thickness leads to a ratio between the minimum creep rate under synthetic air and hydrogenated argon expressed as follows:

(3)
$$k = \frac{\dot{\varepsilon}_{\text{air}}}{\dot{\varepsilon}_{\text{ArH}_2}} = \left(\frac{1 - \alpha \cdot e_{\text{ArH}_2}}{1 - \alpha \cdot e_{\text{air}}} \right)^N.$$

This relation can be used to determine the difference of thickness between the depleted zones ($\Delta e = e_{\text{air}} - e_{\text{ArH2}}$), which might explain the experimental results. With a value of k equal to 5, which is representative of the results obtained, $\Delta e = 75$ μm. This value is much greater than the average measured value which is close to 10 μm (Fig. 12(a)). As shown in Fig. 12(b), localized thicker depleted zones are observed on the specimen tested under synthetic air. Nevertheless the occurrence of these observations is rare and therefore no significant effect on the creep strain rate is expected.
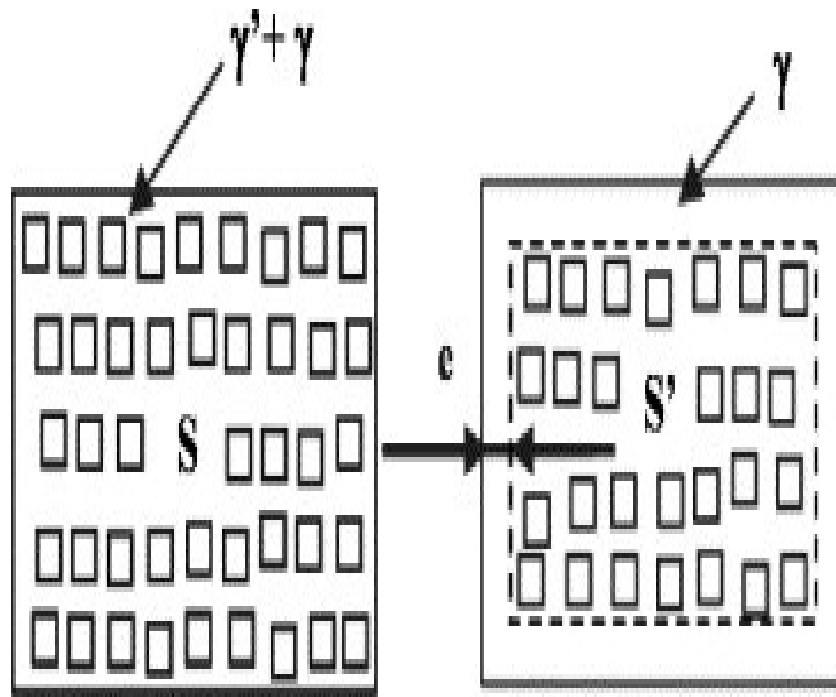
Fig. 13. Scheme of the bearing section decrease due to the depleted zone *e*.

Consequently, we can state that the deleterious effect of oxidation, highlighted by the higher minimum creep rates measured after creep test under synthetic air versus hydrogenated argon, is not mainly due to the development of a γ' depleted zone. Therefore, a longer range effect phenomenon such as the injection of point defects must affect the superalloy creep properties.

3.3. Dynamic effect of oxidation on creep properties

To better understand the way the injection of point defects is likely to affect the creep strain rate, two other kinds of creep tests have been performed: the first one was started under hydrogenated argon and carried out up to the secondary creep stage, and then the atmosphere was changed to dry air until rupture. The second one has been conducted under dry air up to the steady state creep stage and finished under hydrogenated argon. In each case, before switching the environment, a primary vacuum was made to ensure a faster atmosphere transition.

In Fig. 14, the two previous creep curves are superposed on the ones arising from creep tests with a change of atmosphere during the secondary creep stage.
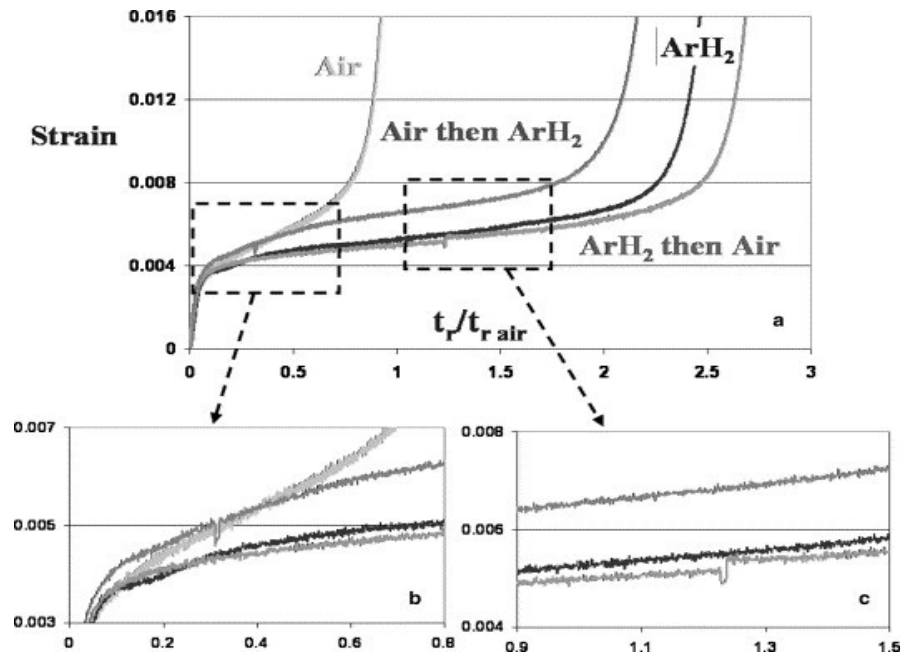
Fig. 14. Normalized creep curves obtained at 1150 °C-σ_0 MPa under different atmospheres: (a) complete curves; (b) and (c) enlargements around atmosphere switches.

3.3.1. Change from ArH_2 to synthetic air

Fig. 14(c) shows that the change of atmosphere, from hydrogenated argon to synthetic air, has no consequence for the creep strain rate.

The oxide layer and the depleted zone are also very similar to the ones observed after the test performed under hydrogenated argon (Fig. 15).
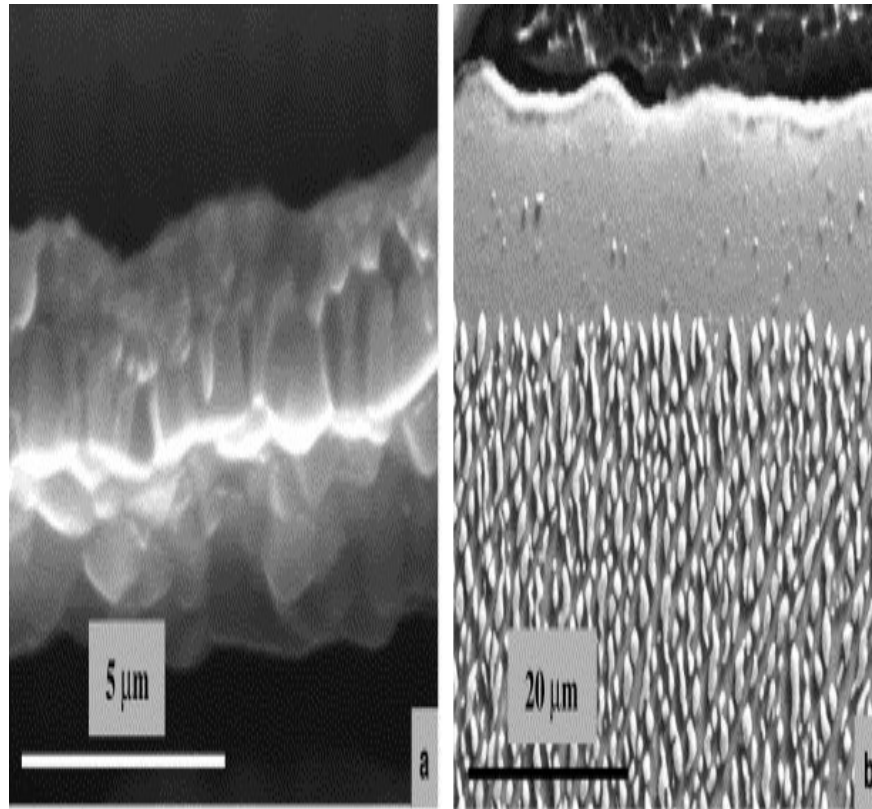
Fig. 15. Micrographs of the specimen after creep test began under hydrogenated argon and finished under synthetic air.

3.3.2. Change from synthetic air to ArH$_2$

Contrary to the previous atmosphere switch, the change from synthetic air to hydrogenated argon (Fig. 14(b)) leads to a progressive decrease of the creep rate until a new equilibrium is reached with a minimum creep rate 2 or 3 times lower (two tests were performed) than before the change. The micrographs in Fig. 16 show that the feature of the oxide scale formed during this kind of tests is intermediate between the oxide microstructure formed under air and under hydrogenated argon. The duplex oxide layer is composed of an inner alumina scale and an outer scale rich in Al, Ni, Cr and Ti. The thickness of the depleted zone varies from 15 to 20 μm but there is no peak up to 60 μm like in the test carried out under synthetic air.
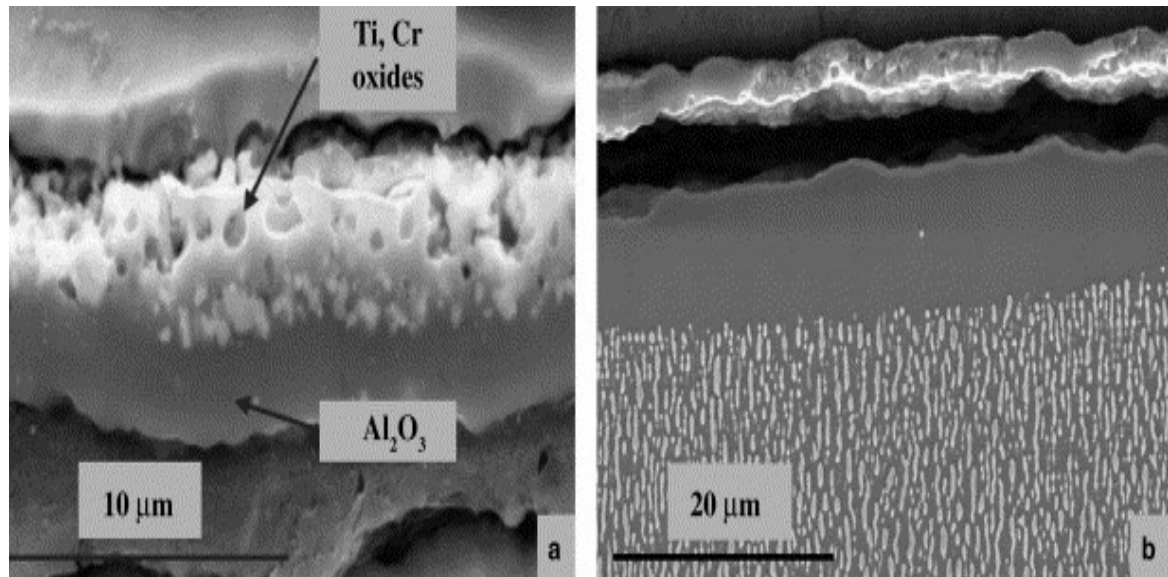
Fig. 16. SEM micrographs: (a) depleted zone of the specimen crept first under synthetic air and then under hydrogenated argon; (b) oxide layer of the specimen crept first under hydrogenated argon and then under synthetic air.

The decrease of the creep rate after changing the atmosphere from synthetic air to hydrogenated argon proves that oxidation has a "dynamic effect" on the superalloy creep strain rate.

The injection of defects is indeed likely to alter the microstructure far from the surface. It leads to a larger affected zone than the observed γ' depleted one and the appearance of a mechanical properties gradient from the surface to the bulk material. If the creep strain rate depends on this mechanical properties gradient, then its decrease after the atmosphere switch would mean that the microstructure is partly recovering. The change in oxidation conditions can slow down the oxidation kinetics, the consumption of aluminum and the injection of defects, but it cannot lead to such a recovery process.

Therefore, there must be a dynamic interaction between the defects injection due to oxidation and the creep mechanisms such as rafting and dislocation motion.

4. Discussion

4.1. Stress effect on the oxide growth

The comparison between thermogravimetric tests and creep tests indicates that the applied stress influences the morphology and the composition of the oxide scale formed under synthetic air. The intensive oxidation during creep test performed under synthetic air explains the higher creep rate under this atmosphere in comparison with the test performed under hydrogenated argon.

The increase of stress level in the growing oxide scale has been clearly established [18] and [19] and could be linked to epitaxial relationships between oxide and metal or to the constraint of a lateral growth strain [20] and [21]. The creep deformation of the specimen under synthetic air probably results in the modification of the stress state in the oxide layer. Thus, during creep testing,

other ways to relax this stress are involved such as wrinkling [22], [23], [24] and [25] or cracking of the oxide layer. In the case of wrinkling, the adherence of the oxide layer may be affected and cracking leads to the formation of transient oxides during the whole test duration (Fig. 11(b)).

The oxide layer under hydrogenated argon stays slightly convoluted even when a tensile stress is applied. The growth of transient oxides under synthetic air may affect the stress state in the oxide layer and intensify undulation [24]. Another explanation of the different stress states could come from a better adhesion of the oxide scale formed under hydrogenated argon than under synthetic air. Looking at the surface of the metal where the oxide scale has spalled (Fig. 17), we can indeed notice that under air there are areas with no imprint left by the alumina grains, which indicates that the oxide scale debonded during the test.
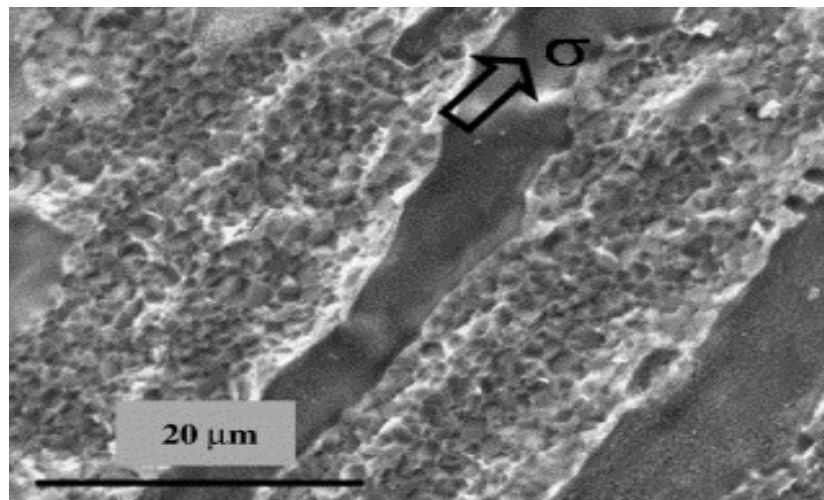

Fig. 17. SEM micrographs of the specimen after creep testing under synthetic air: superalloy surface after spalling.

4.2. Oxidation effect on the creep properties of the single crystal superalloy

We have seen that the oxidation affected zone thickness is not sufficient to explain the difference in creep rate according to the atmosphere, and another dynamic mechanism, such as the injection of defects, must act on creep rate. Studies [26], [27] and [28] have shown that the formation of an oxide scale by outward cationic diffusion towards the external surface of the substrate might induce vacancies injection into the alloy and accelerate diffusion processes.

Cavities were observed just below the surface of all the specimens (Fig. 18(a)). In the micrograph in Fig. 18(b), coming from a previous creep test performed under air with the same kind of specimen and for the same mechanical loading, one can notice that these porosities are not casting porosities aligned along the solidification direction. Hancock [8] and Hales and Hill [29] considered the appearance of these cavities as proof of the injection of vacancies.
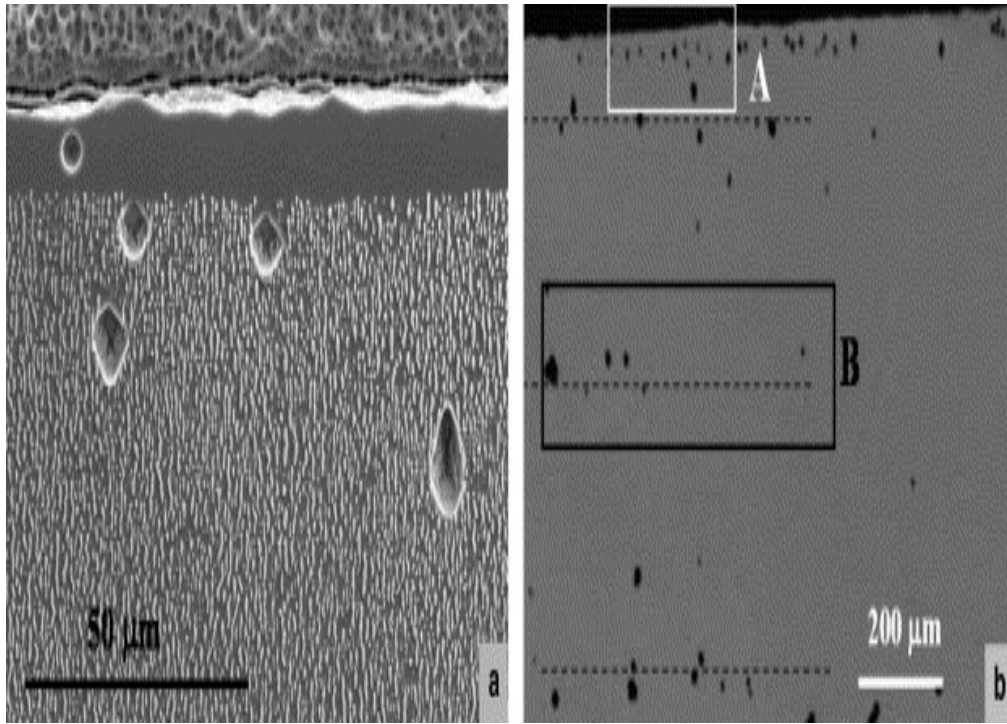
Fig. 18. (a) Micrographs of porosities at the surface of the specimen after creep testing under synthetic air; (b) micrograph showing the difference between porosities just below the surface (A) and casting porosities (B) in the interdendritic areas.

In single crystal superalloy, diffusion is involved in two main creep mechanisms: dislocation climb to bypass γ' particles [30], and morphological changes of γ' precipitates by migration of γ/γ' interfaces [31] and [32]. Oxidation may then have a permanent or "static" effect on creep rate with enhancing microstructure degradation, and a "dynamic" effect with the acceleration of dislocation motion by promoting climbing. These two effects are linked and lead to higher creep rates and shorter times to rupture.

4.3. Comments on creep curves obtained according to the atmosphere

4.3.1. Primary creep stage

Under synthetic air, the application of a stress prevents the formation of a protective alumina scale. The secondary creep stage state is quickly reached but the steady state stage of oxidation is probably not established and transient oxides are still growing. The growth of transient oxides generates a noticeable injection of vacancies which accelerates γ' morphological evolution. Thus, the rafting morphology of precipitates is well established at the end of the primary creep stage.

Under hydrogenated argon, the equilibrium between strain-hardening and recovery is delayed because time is required to establish the steady state stage of oxidation and the γ' evolution from cuboids to quite stable rafts is not enhanced by injection of vacancies.

4.3.2. Steady state creep stage

Under hydrogenated argon, a slow growing and stable alpha alumina scale is formed and the oxidation steady state stage is established. Thus, the change from hydrogenated argon to synthetic air has no effect since the parabolic rate constants are the same under the two atmospheres (Fig. 6).

Under synthetic air, transient oxides are formed. The change from synthetic air to hydrogenated argon leads to a halt in the growth of transient oxides which are not stable in such low oxygen partial pressure. Therefore, the creep rate decreases. The comparison between the curve coming from this test and the one resulting from the test performed under hydrogenated argon provides another piece of information: for the same strain, but not the same duration since damaging kinetics is faster under synthetic air, the creep rates are very similar (Fig. 19). This observation seems to indicate that under synthetic air, the microstructural evolution is accelerated but the γ' morphological change remains the same. That is to say, the microstructural evolution is a creep strain rate controlling parameter, for a given oxidation mechanism.
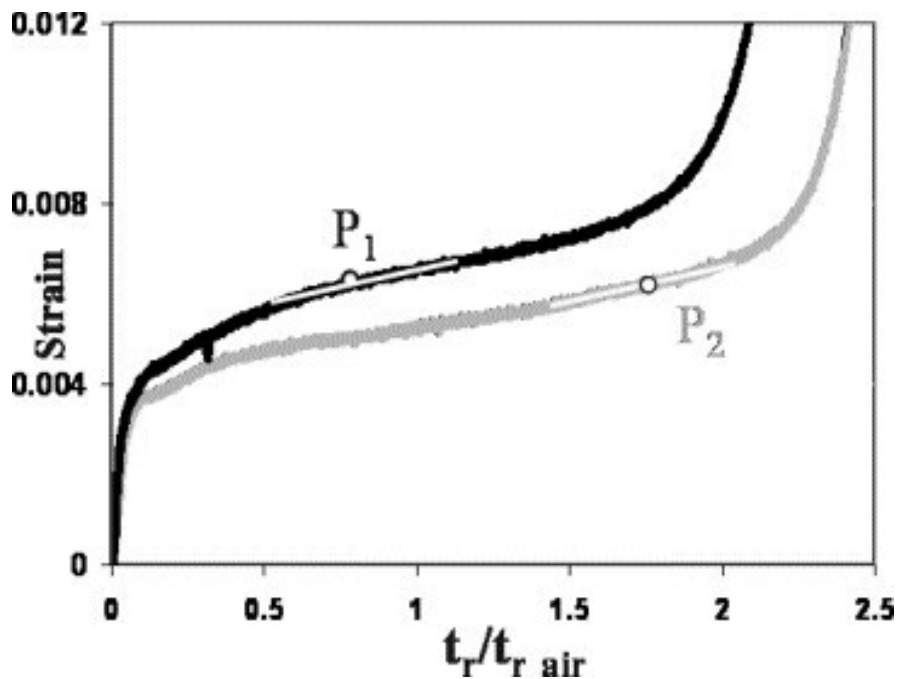

Fig. 19. Comparison of creep rates between the test performed under hydrogenated argon and the one begun under synthetic air and finished under hydrogenated argon.

4.3.3. Tertiary creep stage

The tertiary stage begins with the same critical deformation whatever the atmosphere is. The very fast microstructural degradation leads to a drastic creep rate acceleration. The deleterious effect of oxidation is then no longer perceptible.

The oxide layer formed during the tests performed under hydrogenated argon and the ones with the change from hydrogenated argon to synthetic air are very similar. It indicates that even during the

tertiary stage, there is no cracking or spalling of the oxide layer due to high deformation and high strain rate.

4.4. Integration of oxidation effect in creep strain models

The most convenient way to integrate the deleterious effect of oxidation in creep strain models relies on two main assumptions:

• the increase of creep strain rate is due to the development of a non-load-bearing oxidation affected zone,

• the thickness evolution of the oxidation affected zone depends on the oxidation kinetics rate.

When the oxidation mass gain versus time is given by a linear or a parabolic law, the creep strain rate may then be expressed as follows:

$$\dot{\varepsilon} = \dot{\varepsilon}_0 \left(\frac{\sigma}{1 - \alpha \cdot (e_0 + f(t))} \right)^N \quad \text{with } f(t) = k \cdot t \text{ or } k' \sqrt{t}.$$

The present study is proof that this kind of model is not relevant in the case of single crystal superalloy tested at very high temperature. Oxide scale observations indeed highlight the stress dependence of the oxidation kinetics. Therefore, the data collected by means of the usual oxidation experiments such as thermogravimetric testing are not sufficient. The characterization of specimen microstructure after creep testing does not seem a better solution since the development of the γ' depleted zone is not the main factor in creep resistance degradation. One way may be to consider an equivalent affected zone which is not related to observable microstructural changes. However, extrapolations to predict lifetime components will then be limited to a range of temperatures and stresses for which both oxidation and creep mechanisms remain the same. The injection of vacancies indeed affects the dislocation motion when the controlling mechanism is the bypass of γ' precipitates but this defects injection may, for example, have no effect on precipitates shearing.

Gourgues and Andrieu [33] proposed a new way to integrate in flow laws the oxidation effect they noted on the creep properties of Ni–20Cr thin foil specimens. They considered that the injection of vacancies affects the diffusion coefficient and therefore the $\dot{\varepsilon}_0$ parameter of the Norton power law. This approach is likely to be appropriate in our case with a $\dot{\varepsilon}_0$ parameter depending on the oxidation conditions and the applied stress.

5. Conclusion

The tests performed under controlled atmosphere have shown the drastic oxidation effect on creep properties of a nickel base single crystal superalloy at 1150 °C. This effect is not due to a poor oxidation resistance of the superalloy but to the applied stress which modifies the composition and the morphology of the oxide scale under synthetic air. The decrease of the minimum creep rate after switching the atmosphere from synthetic air to hydrogenated argon proves that this effect of oxidation is not mainly due to the development of a non-load-bearing γ' depleted zone. On the contrary, all the results and observations are consistent with another model stating that oxidation leads to the injection of vacancies in the substrate alloy. This long range phenomenon has a static or permanent effect by altering the microstructure and thus creating a mechanical properties gradient from the surface to the bulk material. The injection of vacancies also has a dynamic effect since it acts on creep mechanisms by promoting dislocation climbing.

References

D.A. Woodford, *Metall Trans A* 12 (1981), p. 299.

M.C. Pandey, *Mater High Temp* 10 (1992) (4), p. 260.

Calvarin-Amiri, A.F. Gourgues, A.M. Hunzt and R. Molins, *Mater Sci Eng A* 298 (2001) (1/2), p. 200.

D.V.V. Satyanarayana, G. Malakondaiah and D.S. Sarma, *Metall Mater Trans A* 34 (2003), p. 2579.

B.F. Dyson and S. Osgerby, *Mater Sci Technol* 3 (1987), p. 545.

N. Roy, R.N. Ghosh and M.C. Pandey, *ISIJ Int* 41 (2001) (8), p. 915.

K.L. Lee, *Composites A* 34 (2003) (12), p. 1235.

Hancock P. In: Proceedings – Met soc conf, vacancies; 1977. p. 215.

E. Andrieu, B. Pierragi and A.F. Gourgues, *Scr Mater* 39 (1998) (4/5), p. 597.

P.J. Ennis, W.J. Quadakkers and H. Schuster, *Mater Sci Technol* 8 (1992), p. 78.

M.C. Pandey, D.M.R. Taplin and P. Ramarao, *Mater Sci Eng A* 118 (1989), p. 33

M. Doner and J.A. Heckler In: S. Reichman, D.N. Duhl, G. Maurer, S. Antolovitch and C. Lund, Editors, *Superalloys 1988*, TMS, Warrendale (PA, USA) (1988).

Dryepondt S, Andrieu E, Monceau D, Crabos F, Vernault C. In: Proceedings – Materials lifetime science and engineering. TMS Annual Meeting, San Diego; 2003.

D. Monceau and B. Pierragi, *Oxidation Met* 50 (1998) (5/6), p. 477.

K. Bouhanek, D. Oquab and B. Pieraggi, *Mater Sci Forum* 251–254 (1997), p. 33.

T. Khan and P. Caron, *Mater Sci Technol* 2 (1996), p. 183.

R.C. Reed, N. Natan, D.C. Cox, A. Rist and C.M.F. Rae, *Acta Mater* 47 (1999) (12), p. 3367.

Evans, *Symp Internal Stresses Met Alloys* (1947), p. 291.

J. Stringer, *Corros Sci* 10 (1970), p. 513.

H.E. Evans, *Int Mater Rev* 40 (1995) (1).

D.R. Clarke, *Acta Mater* 51 (2003), p. 1393.

F.A. Golightly, F.H. Stott and G.C. Wood, *Oxidation Met* 10 (1976) (3), p. 163.

V.K. Tolpygo and R. Clarke, *Acta Mater* 46 (1998) (14), p. 5153.

Z.G. Yang and P.Y. Hou, *Mater Sci Eng A* 391 (2005), p. 1.

ox and G.J. Tatlock, *Mater Sci Technol* 4 (1988), p. 339.

R. Francis and D.G. Lees, *Mater Sci Eng A* 120 (1989), p. 97.

R. Peraldi, D. Monceau and B. Pierragi, *Mater Sci Forum* 369–372 (2001), p. 189.

S. Perusin, B. Viguier, D. Monceau, L. Ressier and E. Andrieu, *Acta Mater* 52 (2004), p. 5375.

R. Hales and A.C. Hill, *Corros Sci* 12 (1972), p. 843.

Fredholm A. PhD thesis, Ecole des Mines de Paris; 1987.

F.R.N. Nabarro, *Scr Mater* 37 (1997) (4), p. 497.

F. Louchet and A. Hazotte, *Scr Mater* 37 (1997) (5), p. 589.

A.F. Gourgues and E. Andrieu, *J Phys IV (France)* 9 (1999) (Pr. 9), p. 297.

Corresponding author. Present address: Metals and Ceramics Division, Oak Ridge National Laboratory, One Bethel Valley Road, Bldg. 4500, P.O. Box 2008, MS-6156, Oak Ridge, TN 37831, United States. Tel.: +1 865 241 5158; fax: +1 865 241 0215.

[1] Present address: Materials Science and Engineering, UNSW, Sydney, Australia.